ChemSusChem

Full Papers
doi.org/10.1002/cssc.202002279

Check for updates

Chemistry
Europe
European Chemical
Societies Publishing

Precious Metal-Free Photocatalytic Water Oxidation by a Layered Double Hydroxide-Prussian Blue Analogue Hybrid Assembly

Sina Sadigh Akbari[a] and Ferdi Karadas*[a, b]

The development of earth-abundant photocatalytic assemblies has been one of the bottlenecks for the advancement of scalable water splitting cells. In this study, a ZnCr layered double hydroxide and a CoFe Prussian blue analogue are combined to afford an earth-abundant photocatalytic assembly involving a visible light-absorbing semiconductor (SC) and a water oxidation catalyst (WOC). Compared to bare ZnCr-LDH, the SC-WOC hybrid assembly exhibits a threefold enhancement in photocatalytic activity, which is maintained for 6 h under photocatalytic conditions at pH 7. The band energy diagram was extracted from optical and electrochemical studies to elucidate the origin of the enhanced photocatalytic performance. This study marks a straightforward pathway to develop low-cost and precious metal-free assemblies for visible light-driven water oxidation.

Introduction

Photocatalytic water oxidation with powder suspensions has been an appealing strategy since it offers a simple, relatively low-cost, and easily scalable method to harvest solar light. These photocatalytic assemblies generally involve the coupling of a suitable semiconductor (SC) with a water oxidation catalyst (WOC).[1,2] Although hundreds of different assemblies have been reported up to date, the majority of them are active mostly in the UV region (<400 nm), and/or WOCs are mainly based on precious metal oxides.[3–5] Therefore, the development of an earth-abundant and visible-light absorbing SC-WOC assembly is one of the critical challenges for the advancement of scalable and efficient photocatalytic water splitting systems.

Layered double hydroxides (LDHs) consisting of mixed-metal hydroxide layers step forward in photocatalytic water splitting due to their simple synthesis, diversity, abundant active earth-metal centers, and efficient visible light-harvesting properties.[6–13] Although LDHs have been actively used for photocatalytic water splitting due to their high quantum yield and efficiency, only a limited number of studies involve the utilization of ZnCr-LDH as a narrow bandgap semiconductor for the photocatalytic water oxidation process.[14] ZnCr-LDH has been employed either as an individual photocatalyst[15–17] or as part of a heterostructure consisting of a combination of suitable semiconductors for overall water splitting.[18–20] Although ZnCr-LDH exhibits a suitable band energy alignment for visible light-driven water oxidation, poor charge mobility in LDHs leads to unavoidable recombination of photo-induced charge carriers, which yields relatively poor efficiency and stability.[14] Therefore, viable strategies to suppress photo-generated electron-hole recombination and to improve the interfacial kinetics of LDH-based materials should be introduced for the advancement of LDH-based water splitting technologies.[21–24] Although ZnCr-LDH has been coupled with other semiconductors for photocatalytic applications, it has not been combined with a water oxidation catalyst up to date.

Such a design requires the coupling of two earth-abundant components with matching band levels for efficient charge separation. Cobalt-iron Prussian blue analogues, CoFe-PBAs, have recently been acknowledged as efficient and robust WOCs. In CoFe-PBAs, cobalt sites, which are coordinated to at least one water molecule, are active catalytic sites while iron sites that are surrounded with six cyanide groups are catalytically inactive.[25–31] Since they exhibit poor photocurrent efficiencies, the general strategy is to couple CoFe-PBAs with suitable photosensitizers and semiconductors to utilize them for the light-driven water oxidation process.[27,32] Herein, we prepare SC-WOC hybrid assembly by coupling a CoFe-PBA with a ZnCr-LDH since i) they are precious metal free, ii) they can be prepared by straightforward solution chemistry, and iii) CoFe-PBAs are projected to have a suitable band energy alignment that can facilitate charge transfer from the valence band of ZnCr-LDH for the water oxidation reaction.[33–36]

[a] S. S. Akbari, Prof. F. Karadas
     Department of Chemistry, Faculty of Science
     Bilkent University, 06800, Ankara (Turkey)
     .
     E-mail: karadas@fen.bilkent.edu.tr
[b] Prof. F. Karadas
     UNAM – National Nanotechnology Research Center, Institute of Materials
     Science and Nanotechnology
     Bilkent University, 06800, Ankara (Turkey)

Results and Discussion

ZnCr-LDHs and CoFe-PBAs have been prepared according to previously reported synthetic methods. The compounds were then mixed at 60 °C with different weight ratios to afford hybrid assemblies symbolized as LDH-PB-n (n = 1, 2, or 3; Figure 1a). All

ChemSusChem

Full Papers
doi.org/10.1002/cssc.202002279

Chemistry Europe
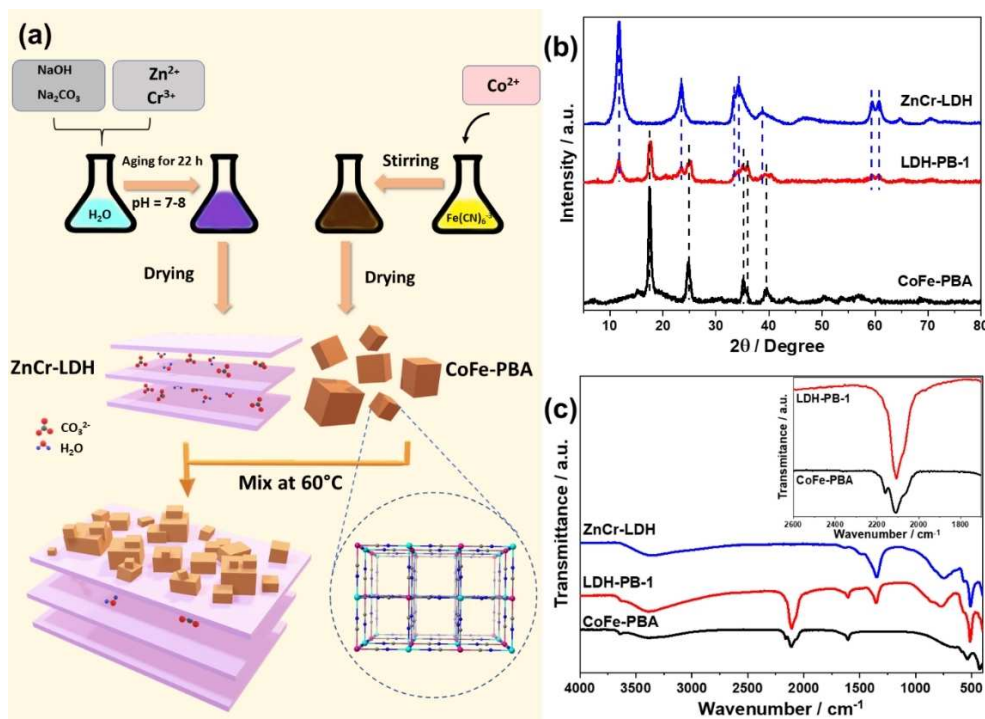European Chemical
Societies Publishing

Figure 1. (a) Schematic representation for the preparation of LDH-PB-n hybrid assemblies by mixing ZnCr-LDH and CoFe-PBA at 60 °C with different weight ratios. (b) XRD patterns of LDH, PBA, and LDH-PB-1. The dashed lines represent the characteristic diffraction peaks for LDH and PBA structures in the powder XRD pattern of the LDH-PB-1 sample. (c) ATR-FTIR spectra of LDH, PBA, and LDH-PB-1. Inset: The cyanide stretching mode for CoFe-PBA and LDH-PB-1 samples.

characteristic peaks of a layered double hydroxide and a Prussian blue structure were observed in powder XRD patterns of samples (Figure 1b and Figure S1 in the Supporting Information). The diffraction peaks at 11.7° and 23.5° that are observed for ZnCr-LDH are assigned to (003) and (006) lattice planes of LDH structure while the ones at 17.5° and 24.8° observed for CoFe-PBA correspond to (200) and (220) lattice planes of cubic Prussian blue structure, respectively (Table S1).[17,37] These peaks are also observed for LDH-PB-1 without any significant shift, which suggests a physical interaction between components in LDH-PB-1. The relative intensities of the diffraction peaks that belong to PB structures in LDH-PB-1 decrease and they get broader compared to CoFe-PBA, which indicates that the particle size is reduced during the formation of the hybrid assembly.

The FTIR spectra for ZnCr-LDH and LDH-PB-n reveal a broad band at 3370 cm^{-1} and a sharp one at 1632 cm^{-1}, which are attributed to the M–O–H stretching mode and the bending mode of H$_2$O. The broadness of the O–H band indicates the presence of hydrogen bonds between water molecules and anions in the interlayer space of LDH. The two bands at 1487 cm^{-1} and 1348 cm^{-1} are assigned to the asymmetric stretching of the carbonate species placed in between the layers. The spectra for CoFe-PBA and LDH-PB-n reveal a sharp band at 2110 cm^{-1} with two shoulders at 2160 cm^{-1} and 2070 cm^{-1}, which are assigned to Co^{III}–NC–Fe^{II}, Co^{II}–NC–Fe^{III}, and Co^{II}–NC–Fe^{II} coordination modes, respectively. The relative decrease in the intensity of the shoulder at 2160 cm^{-1} for LDH-

PB-n suggests an electron transfer from LDH to PBA structures (Figures 1c and S2).[38,39]

The morphology and structure of the samples were investigated by scanning electron microscopy (SEM) and Transmission electron microscopy (TEM) images. The layered structure of ZnCr-LDH was confirmed with SEM analysis (Figure 2a),[40] which are surrounded by Prussian blue structures after mixing to produce hybrid assemblies (Figure 2b,c). The morphology of LDH-PB-1 has also been investigated with TEM analysis since it exhibits the highest photocatalytic water oxidation performance (Figure 2d). Scanning TEM (STEM) elemental mapping confirms that CoFe-PBA particles are distributed on the surface of LDH layers in LDH-PB-1 (Figures 2e and S3).[18,41,42] Energy-dispersive X-ray spectroscopy (EDS) elemental scanning reveals Co/Fe and Zn/Cr elemental ratios of 3:2 and 2:1, respectively, which is consistent with our synthetic procedure (Figure S4 and Table S2). EDS mapping indicates that the PB and LDH structures are well-dispersed to form a uniform hybrid assembly (Figure S5).

The possible electron transfer between LDH and PBA structures is also observed with X-ray photoelectron spectroscopy studies. The corresponding binding energies for Zn 2p, Cr 2p, Co 2p, Fe 2p, N 1s, C 1s, and O 1s (Figures S6 and S7) are in good accordance with the expected profiles of CoFe-PBA and ZnCr-LDH. A comparison of XPS profiles before and after mixing indicates that the binding energies of Zn 2p and Cr 2p exhibit slightly positive shifts after mixing.[20] Cobalt retains its +2 and +3 oxidation states,[35,43,44] whereas the amount of Fe^{2+} ions in

ChemSusChem

Full Papers
doi.org/10.1002/cssc.202002279

**Chemistry
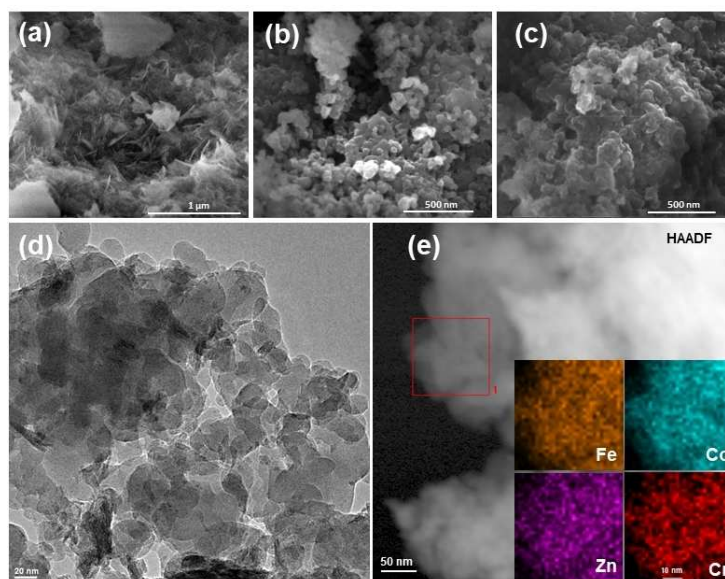Europe**
European Chemical
Societies Publishing

Figure 2. SEM images of (a) ZnCr-LDH, (b) CoFe-PBA, and (c) LDH-PB-1. (d) TEM image of LDH-PB-1. (e) High-angle annular dark field (HAADF) image of the LDH-PB-1 sample. Inset shows the selected-area STEM elemental mapping.

the mixed-valent iron sites increases upon mixing suggesting an electron transfer from LDH to PBA structures (Figures 3 and S8),[27] which is in agreement with FTIR profile of LDH-PB-1 sample.

The photocatalytic performances of bare LDH and LDH-PB-*n* samples were evaluated by monitoring the amount of gen-

erated oxygen from water in the presence of 5 mM $Na_2S_2O_8$ as a sacrificial agent under visible-light irradiation (Figures 4a and S9). ZnCr-LDH exhibits a considerable photocatalytic activity, which decreases gradually in the second cycle (0.64 mmol g^{-1} h^{-1}). LDH-PB-1 exhibits a threefold increase in the activity (1.83 mmol g^{-1} h^{-1}) compared to bare ZnCr-LDH and
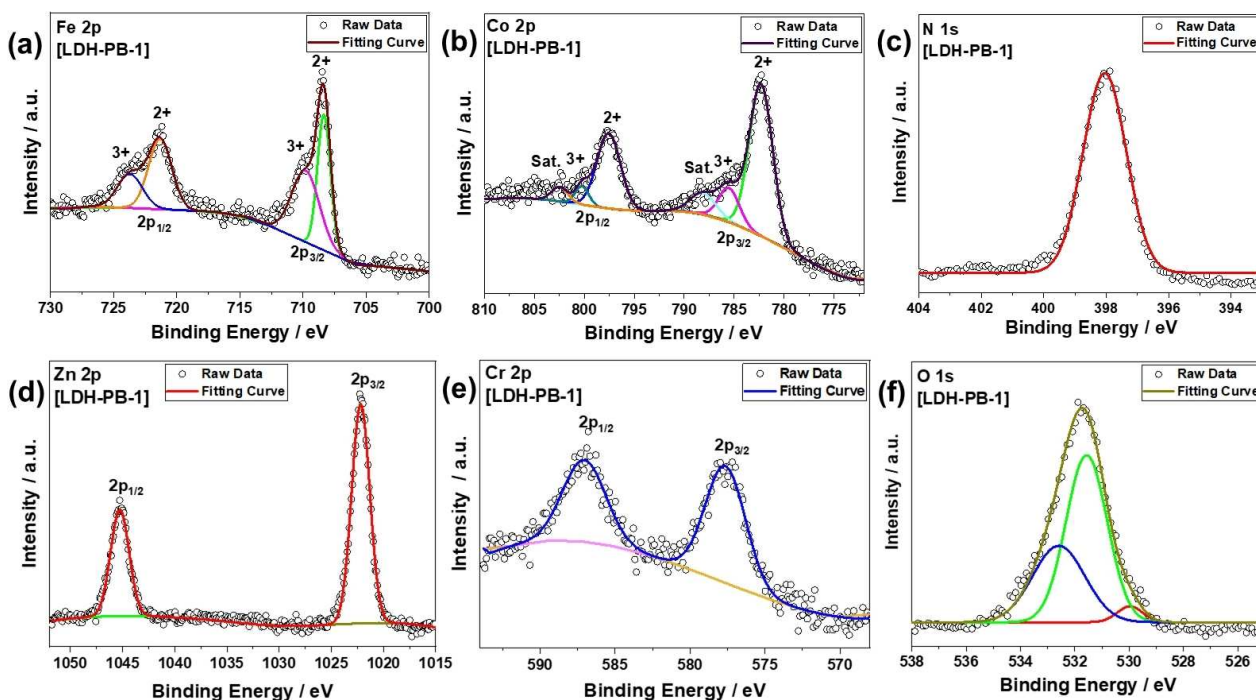

Figure 3. XPS spectra of the LDH-PB-1 sample: (a) Fe 2p; (b) Co 2p; (c) N 1s; (d) Zn 2p; (e) Cr 2p; (f) O 1s. Circles and lines represent raw data and fitted curves, respectively.
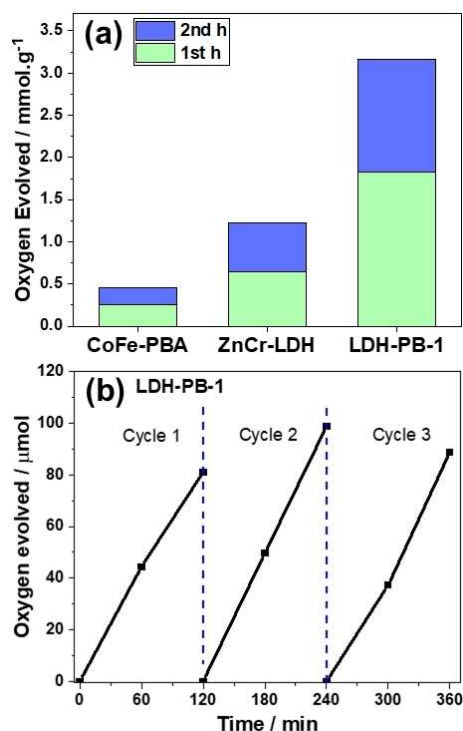
ChemSusChem

Full Papers
doi.org/10.1002/cssc.202002279

**Chemistry
Europe**

European Chemical
Societies Publishing

Figure 4. (a) Bar diagrams of photocatalytic O_2 evolution of CoFe-PBA, ZnCr-LDH, and LDH-PB-1 (mmol of produced O_2 per g of catalyst) in a pH 7 KPi buffer containing 5 mM $Na_2S_2O_8$ as a sacrificial agent under visible-light irradiation ($\lambda > 420$ nm). (b) Rate of O_2 generation in 3 consecutive cycles for LDH-PB-1. After each cycle 5 mM $Na_2S_2O_8$ was added to the reaction solution.

CoFe-PBA, which maintains its activity even during the third cycle (Figure 4b). The trend in the photocatalytic activity clearly shows that coupling a PBA structure as a WOC not only enhances the activity but also the stability of LDH structures under photocatalytic conditions. The highest photocatalytic activity and stability were obtained when the LDH/PBA molar ratio was 1:1 (LDH-PB-1), which maintains its activity during a 6 h photocatalytic experiment. When the molar amount of the LDH component is twice that of the PBA one (LDH-PB-2), the activity decreases to approximately half its value (0.64 mmol g^{-1} h^{-1}), which could be attributed to the decrease in the weight ratio of the catalyst in the assembly. For LDH-PB-3, which has a molar ratio of 2:3, the activity is ca. 0.87 mmol g^{-1} h^{-1} in the first cycle. The activity of LDH-PB-3 in the second cycle is, however, poorer (0.63 mmol g^{-1} h^{-1}) due to a possible photodecomposition. The lower stability in LDH-PB-3 could be attributed to a higher degree of aggregation of excess PB particles, which leads to a relatively inefficient electron transfer between components. Furthermore, the physically mixed LDH+PBA sample displays a similar activity to LDH-PB-1 over the first cycle, which decreases significantly in the second cycle (Figure S10) due to the decomposition of the LDH structure as evidenced by post-catalytic XRD studies (Figure S11). These studies indicate that both the synthetic method and the molar ratio of the components play an important role in tuning the physical interaction between the components

and, thus, in the activity and photostability. We also studied the effect of the sacrificial agent by evaluating the photocatalytic activity of ZnCr-LDH and LDH-PB-1 with $AgNO_3$ as well. Whereas ZnCr-LDH exhibits a similar activity in the presence of different sacrificial agents, the activity of LDH-PB-1 depends highly on the type of electron scavenger. The activity of LDH-PB-1 is around two times higher in $S_2O_8^{2-}$ compared to $AgNO_3$ since persulfate anion produces an intermediate sulfate radical ($SO_4^{\bullet-}$), which is a strong oxidizing agent (Figure S12).[45]

Turnover frequency (TOF) is also an important indicator to compare the activity of the catalytic sites, which is defined as the number of O_2 or H_2 per catalytic active site per time.[46] For the estimation of the lower-bound TOF value, a rough molecular formula was extracted from EDX analysis and all the cobalt sites are assumed to be catalytically active. The TOF for LDH-PB-1 is obtained to be around 2.1×10^{-4} s^{-1}, which is comparable to previously reported TOF values for Prussian blue-based systems.[27,33,34]

The band structure and optical properties of ZnCr-LDH, CoFe-PBA, and mixed samples were investigated with UV/Vis diffuse-reflectance spectroscopy (Figures 5a and S13). ZnCr-LDH exhibits two strong bands at 410 and 570 nm corresponding to the $^4A_{2g} \rightarrow ^4T_{1g}$ (F) and $^4A_{2g} \rightarrow ^4T_{2g}$ (F) d–d transitions of chromium ions, respectively.[47,48] The absorption band initiated at 344 nm can be assigned to the ligand to metal charge transfer (LMCT) from the O 2p orbital to the Cr 3d(e_g) and Zn 4s orbitals.[49] When it is coupled with CoFe-PBA, the background absorption of the compound was significantly increased due to the electronic interaction between LDH and PBA structures. Two broad absorption regions in CoFe-PBA can be attributed to the charge transfer in the structure.[50] The enhancement in the photocatalytic activity of the LDH-PB-1 sample is also investigated by photoluminescence spectroscopy (PL). In Figure 5b, ZnCr-LDH displays a remarkable depression of PL peaks upon hybridization with the PBA structure. Taking into account the higher visible light absorption of the LDH-PB-1 sample compared to pristine LDH, the PL results suggest an efficient electron transfer between LDH and PBA components, which could sufficiently suppress the recombination of photo-generated electrons and holes.[14,51]

Cyclic voltammetry (CV) measurements and DRS results were evaluated to estimate the band energy diagram. The literature is contradictory on the assignment of band energy levels of ZnCr-LDH mainly due to the presence of 3d^3 states of Cr^{3+} ions in addition to conduction and valence bands (Table S4). Cyclic voltammetry of ZnCr-LDH is utilized to assign the position for the $^4A_{2g}$ state at 1.92 V vs. NHE, whereas the HOMO level of CoFe-PBA is positioned at 1.48 V vs. NHE (Figure S14). The bandgap of LDH is found to be 3.97 eV based on the fitting of absorption data with the Tauc plot (Figure S15). The HOMO level of PBA is located at a higher energy level compared to the d(t_{2g}) level of LDH (Figure 5c). The electrons in d(t_{2g}) orbitals of LDH are excited to the unoccupied interband states by absorbing visible light. As a result, the photo-generated holes can be injected into the HOMO level of PBA, which causes an efficient charge separation.
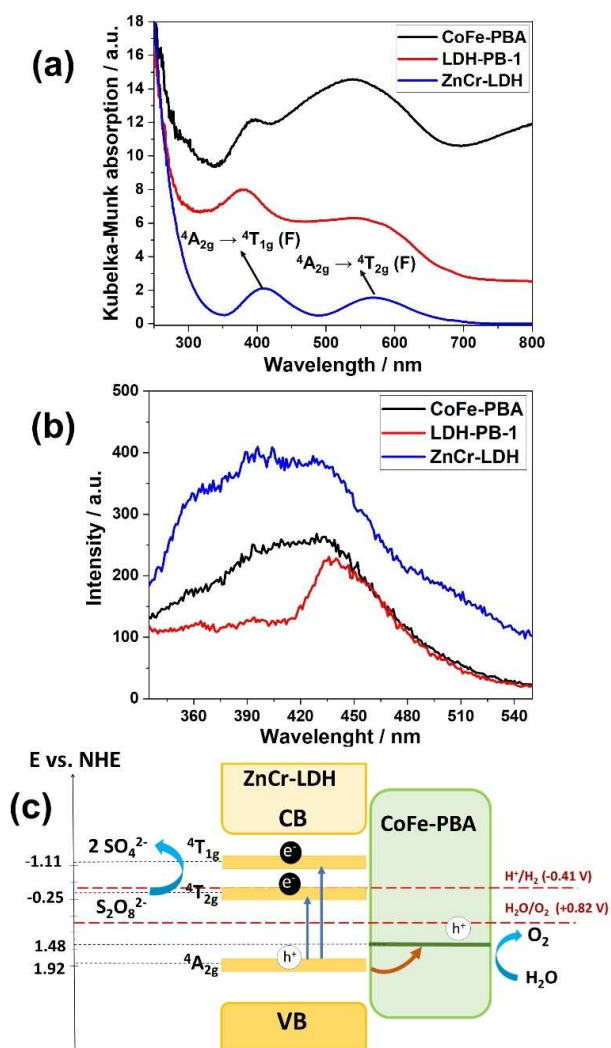
ChemSusChem

Full Papers
doi.org/10.1002/cssc.202002279

**Chemistry
Europe**
European Chemical
Societies Publishing

Figure 5. (a) Diffuse-reflectance UV/Vis spectra (plotted as the Kubelka–Munk function of the reflectance, R) of CoFe-PBA, ZnCr-LDH, and LDH-PB-1 samples in the 250–800 nm wavelength range. (b) PL spectra of CoFe-PBA, ZnCr-LDH, and LDH-PB-1 samples ($\lambda_{ex} = 290$ nm) at room temperature. (c) Schematic representation of the estimated band structure of the LDH-PB-1 sample (pH 7) involving the electron-transfer mechanism.

The robustness of the hybrid assembly is elucidated with XPS and XRD studies performed on post-catalytic powder samples. For the Cr 2p and Zn 2p peaks, a slight shift to higher binding energy was observed. The corresponding Fe^{3+} peaks are diminished significantly, whereas those for Fe^{2+} remain unchanged. These results support the thesis that the electron transfer takes place between LDH and PBA during the photocatalytic water oxidation process, which reduces Fe^{3+} to Fe^{2+}. No significant change in the Co 2p profile is observed in pristine and post-catalytic samples indicating the stability of the Co^{2+} sites (Figure 6a–d).

XRD patterns were also studied for pristine and post-catalytic powder samples of CoFe-PBA, ZnCr-LDH, and LDH-PB-1. Similar to previous studies, the CoFe-PBA sample was observed to be stable during the photocatalytic water oxidation process based on the comparison of XRD profiles of pristine

and post-catalytic CoFe-PBA samples (Figure 6e). ZnCr-LDH, however, exhibits additional peaks in the post-catalytic sample, which reveals that it decomposes partially to K_2Zn_4O-$(CrO_4)_4 \cdot 3H_2O$ under photocatalytic conditions (Figure 6f). The decrease in the activity of ZnCr-LDH in the 2nd cycle could thus be attributed to its low stability. For LDH-PB-1, all the peaks obtained in the pristine and post-catalytic samples correspond to those for PB cubic and LDH structures (Figure 6g). It should be noted that a possible decomposition to an amorphous structure cannot be ruled out merely based on XRD studies. The steady profile of the photocatalytic activity throughout several cycles with LDH-PB-1 and XRD studies performed on pristine and post-catalytic CoFe-PBA, ZnCr-LDH, and LDH-PB-1 samples reveal that the LDH structure exhibits a remarkable enhancement in the stability once it is coupled with CoFe-PBA to form LDH-PB-1. No additional peaks that can be attributed to a decomposed product are observed in the Infrared spectra of pristine and post-catalytic samples for ZnCr-LDH and LDH-PB-1 (Figure S16). The FTIR spectra of LDH-PB-1 sample before and after the photocatalytic experiment show an electron transfer process between LDH and PBA, which is consistent with XPS studies.

Conclusions

In summary, the strengths of layered double hydroxides and Prussian blue structures were combined to develop an entirely earth-abundant semiconductor–catalyst assembly for the visible light-driven water oxidation process. We changed experimental parameters including the mixing temperature and weight ratio of components systematically and optimized the synthetic methodology to obtain a combination of enhanced activity and stability. The summary of photocatalytic performances of previously reported ZnCr-LDHs (listed in Table S5) indicates that the LDH-PB assembly exhibits a remarkable activity among LDH-based systems. ZnCr-LDH serves as an efficient visible light-absorbing semiconductor, whereas CoFe-PBA plays an active role in the catalytic water oxidation process. The photocatalytic assembly is easy to prepare and is composed of earth-abundant components. The well-placed energy level of CoFe Prussian blue structure between the water oxidation and the valence band of ZnCr-LDH makes it an ideal catalyst for efficient hole transfer from the semiconductor to the water oxidation process. This efficient electron transfer not only reveals a threefold enhancement in photocatalytic performance compared to bare LDH but also improves its stability under photocatalytic conditions. We also observed that the molar ratio of LDH and PB components can be tuned to enhance the activity and stability of LDH-PB assemblies. Given the remarkable photocatalytic performance of this hybrid assembly and the diversity in both the layered double hydroxide and Prussian blue chemistry, a systematic study on the overall water splitting with LDH-PB assemblies is currently underway.
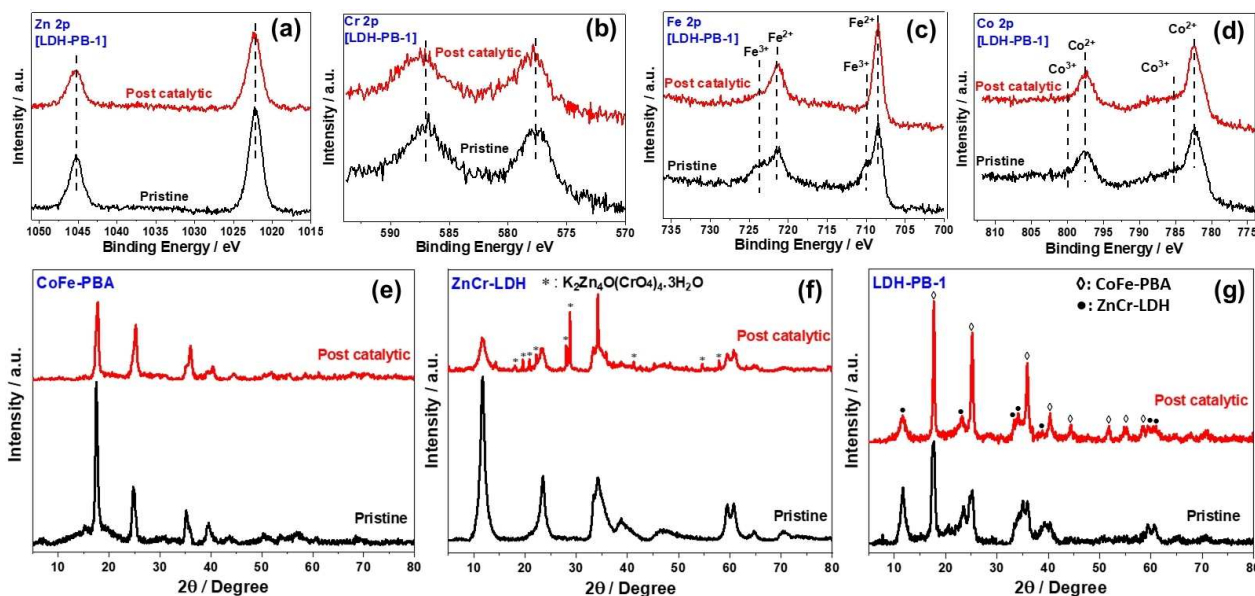
ChemSusChem

Full Papers
doi.org/10.1002/cssc.202002279

Chemistry Europe
European Chemical
Societies Publishing

Figure 6. XPS spectra of (a) Zn 2p, (b) Cr 2p, (c) Fe 2p, and (d) Co 2p for pristine (black line) and post-catalytic (red line) of LDH-PB-1 sample. XRD patterns of (e) CoFe-PBA, (f) ZnCr-LDH, and (g) LDH-PB-1 for pristine (black line) and post-catalytic (red line) samples.

Experimental Section

Synthesis of ZnCr-LDH

The co-precipitation method was used for the synthesis of ZnCr-LDH, similar to the reported procedure with slight modifications.[18] $Zn(NO_3)_2 \cdot 6H_2O$ and $Cr(NO_3)_3 \cdot 6H_2O$ with a Zn/Cr molar ratio of 2:1 were dissolved in deionized water (30 mL; solution A). Then, solution A was titrated with another solution containing 1 M NaOH and 1 M Na_2CO_3 (solution B) until pH 7–8 was reached under vigorous stirring at room temperature. The resultant suspension was stirred for 4 h. Subsequently, the mixture was aged at 85 °C for 22 h. The purple slurry was separated by centrifugation, rinsed with deionized water, and finally dried at 75 °C

Synthesis of CoFe-PBA

CoFe-PBA was synthesized by a precipitation method.[37] First, $K_3[Fe(CN)_6]$ (2 mmol) was dissolved deionized water (20 mL). Then, an aqueous solution of $Co(NO_3)_2 \cdot 3H_2O$ (3 mmol in 20 mL water) was added dropwise to the above solution at room temperature. The obtained slurry was stirred for 1 h and left to stand overnight. The final precipitate was collected by centrifugation and washed thoroughly with water. The obtained solid was dried at 75 °C.

Synthesis of LDH-PBA mixture

For the preparation of LDH-PBA assemblies, LDH and PBA powder samples with specific quantities were separately dispersed in a water/ethanol (1:1 v/v) mixture and sonicated for 30 min. Then, solutions were mixed with ultrasonication for 2 h. Subsequently, the mixture was stirred at 60 °C for 6 h (Figure 1a). The resulting materials with 1:1, 2:1, and 2:3 weight ratios are denoted as LDH-PB-1, LDH-PB-2, and LDH-PB-3, respectively.

Photocatalytic Experiments

The photocatalytic experiments for oxygen evolution were performed in a 21 mL Pyrex reactor. Catalysts (28 mg; 14 mg for experiments involving bare PBA and LDH samples) were dispersed in aqueous buffer solution (18 mL; 0.1 M KH_2PO_4 and 0.1 M K_2HPO_4 diluted in 500 mL deionized water with a pH close to 7) containing 5 mM $Na_2S_2O_8$ as a sacrificial agent. The headspace of the flask was sealed with septa and the reaction mixtures were purged thoroughly with N_2 to remove air. A Xe lamp (300 W; AM 1.5 global filter.) with a UV cutoff filter ($\lambda > 420$ nm) was used as a light source. The amount of evolved oxygen was determined by injecting 100 μL of the reactor headspace gas into a gas chromatograph (Agilent 7820 A GC) equipped with a Molesieve column and a TCD detector. Ar was used as the carrier gas. For each sample, photocatalytic tests were repeated 3 to 5 times to achieve reliable results.

Acknowledgements

Conflict of Interest

The authors declare no conflict of interest.

[1] S. J. A. Moniz, S. A. Shevlin, D. J. Martin, Z. X. Guo, J. Tang, *Energy Environ. Sci.* **2015**, *8*, 731–759.

[2] T. Hisatomi, J. Kubota, K. Domen, *Chem. Soc. Rev.* **2014**, *43*, 7520–7535.

[3] S. Berardi, S. Drouet, L. Francàs, C. Gimbert-Suriñach, M. Guttentag, C. Richmond, T. Stoll, A. Llobet, *Chem. Soc. Rev.* **2014**, *43*, 7501–7519.

[4] T. Takata, K. Domen, *ACS Energy Lett.* **2019**, *4*, 542–549.

[5] K. E. Dalle, J. Warnan, J. J. Leung, B. Reuillard, I. S. Karmel, E. Reisner, *Chem. Rev.* **2019**, *119*, 2752–2875.

[6] J. W. L. Yeob Lee, J. K. K. Yeob Lee, Jung Hoon Choi, Hyung Joon Jeon, Kyung Min Choi, *Energy Environ. Sci.* **2011**, *4*, 914–920.

[7] D. S. Su, M. Wei, X. Duan, B. Wang, Y. Zhao, X. Cao, S. Zhang, P. Chen, L. Tian, D. G. Evans, J. Lu, Z. Li, B. Zhang, *Chem. Eur. J.* **2012**, *18*, 11949–11958.

[8] Y. Zhao, B. Li, Q. Wang, W. Gao, C. J. Wang, M. Wei, D. G. Evans, X. Duan, D. O'Hare, *Chem. Sci.* **2014**, *5*, 951–958.

[9] H. Zhou, Y. Song, Y. Liu, H. Li, W. Li, Z. Chang, *Int. J. Hydrogen Energy* **2018**, *43*, 14328–14336.

[10] S. Nayak, K. M. Parida, *Int. J. Hydrogen Energy* **2016**, *41*, 21166–21180.

[11] A. R. Amani-Ghadim, F. Khodam, M. S. Seyed Dorraji, *J. Mater. Chem. A* **2019**, *7*, 11408–11422.

[12] Y. Dou, S. Zhang, T. Pan, S. Xu, A. Zhou, M. Pu, H. Yan, J. Han, M. Wei, D. G. Evans, X. Duan, *Adv. Funct. Mater.* **2015**, *25*, 2243–2249.

[13] S. M. Xu, H. Yan, M. Wei, *J. Phys. Chem. C* **2017**, *121*, 2683–2695.

[14] J. L. Gunjakar, T. W. Kim, H. N. Kim, I. Y. Kim, S. J. Hwang, *J. Am. Chem. Soc.* **2011**, *133*, 14998–15007.

[15] C. G. Silva, Y. Bouizi, V. Fornés, H. García, *J. Am. Chem. Soc.* **2009**, *131*, 13833–13839.

[16] K. Parida, L. Mohapatra, *Dalton Trans.* **2012**, *41*, 1173–1178.

[17] Y. Fu, F. Ning, S. Xu, H. An, M. Shao, M. Wei, *J. Mater. Chem. A* **2016**, *4*, 3907–3913.

[18] D. P. Sahoo, S. Nayak, K. H. Reddy, S. Martha, K. Parida, *Inorg. Chem.* **2018**, *57*, 3840–3854.

[19] C. Wang, B. Ma, S. Xu, D. Li, S. He, Y. Zhao, J. Han, M. Wei, D. G. Evans, X. Duan, *Nano Energy* **2017**, *32*, 463–469.

[20] D. P. Sahoo, S. Patnaik, K. Parida, *ACS Omega* **2019**, *4*, 14721–14741.

[21] J. L. Gunjakar, I. Y. Kim, J. M. Lee, N. S. Lee, S. J. Hwang, *Energy Environ. Sci.* **2013**, *6*, 1008–1017.

[22] J. L. Gunjakar, T. W. Kim, I. Y. Kim, J. M. Lee, S. J. Hwang, *Sci. Rep.* **2013**, *3*, 2080.

[23] G. Zhang, B. Lin, L. Qiu, L. He, Y. Chen, B. Gao, *Int. J. Hydrogen Energy* **2015**, *40*, 4758–4765.

[24] M. Sohail, H. Kim, T. W. Kim, *Sci. Rep.* **2019**, *9*, 7584.

[25] Y. Yamada, K. Oyama, R. Gates, S. Fukuzumi, *Angew. Chem. Int. Ed.* **2015**, *54*, 5613–5617; *Angew. Chem.* **2015**, *127*, 5705–5709.

[26] F. S. Hegner, I. Herraiz-Cardona, D. Cardenas-Morcoso, N. López, J. R. Galán-Mascarós, S. Gimenez, *ACS Appl. Mater. Interfaces* **2017**, *9*, 37671–37681.

[27] S. Goberna-Ferrón, W. Y. Hernández, B. Rodríguez-García, J. R. Galán-Mascarós, *ACS Catal.* **2014**, *4*, 1637–1641.

[28] Y. Aratani, K. Oyama, T. Suenobu, Y. Yamada, S. Fukuzumi, *Inorg. Chem.* **2016**, *55*, 5780–5786.

[29] L. Han, P. Tang, Á. Reyes-Carmona, B. Rodríguez-García, M. Torréns, J. R. Morante, J. Arbiol, J. R. Galan-Mascaros, *J. Am. Chem. Soc.* **2016**, *138*, 16037–16045.

[30] B. M. Pires, P. L. Dos Santos, V. Katic, S. Strohauer, R. Landers, A. L. B. Formiga, J. A. Bonacin, *Dalton Trans.* **2019**, *48*, 4811–4822.

[31] S. Pintado, S. Goberna-Ferrón, E. C. Escudero-Adán, J. R. Galán-Mascarós, *J. Am. Chem. Soc.* **2013**, *135*, 13270–13273.

[32] T. G. Ulusoy Ghobadi, A. Ghobadi, M. C. Soydan, M. Barzgar Vishlaghi, S. Kaya, F. Karadas, E. Ozbay, *ChemSusChem* **2020**, *13*, 2577–2588.

[33] Z. Kap, F. Karadas, *Faraday Discuss.* **2019**, *215*, 111–122.

[34] T. G. Ulusoy Ghobadi, E. Akhuseyin Yildiz, M. Buyuktemiz, S. Sadigh Akbari, D. Topkaya, Ü. İsci, Y. Dede, H. G. Yaglioglu, F. Karadas, *Angew. Chem. Int. Ed.* **2018**, 17173–17177; *Angew. Chem.* **2018**, *130*, 17419–17423.

[35] T. G. Ulusoy Ghobadi, A. Ghobadi, M. Buyuktemiz, E. A. Yildiz, D. Berna Yildiz, H. G. Yaglioglu, Y. Dede, E. Ozbay, F. Karadas, *Angew. Chem. Int. Ed.* **2020**, *59*, 4082–4090; *Angew. Chem.* **2020**, *132*, 4111–4119.

[36] M. Aksoy, S. V. K. Nune, F. Karadas, *Inorg. Chem.* **2016**, *55*, 4301–4307.

[37] E. P. Alsaç, E. Ülker, S. V. K. Nune, Y. Dede, F. Karadas, *Chem. Eur. J.* **2018**, *24*, 4856–4863.

[38] O. Sato, T. Iyoda, A. Fujishima, K. Hashimoto, *Science* **1996**, *272*, 704–705.

[39] S. J. Gerber, E. Erasmus, *Mater. Chem. Phys.* **2018**, *203*, 73–81.

[40] Y. Xu, L. Tan, Y. Zhao, Y. Song, *Ind. Eng. Chem. Res.* **2020**, *59*, 14315–14322.

[41] Y. Q. Wang, J. Z. Ma, J. Wang, S. Chen, H. S. Wang, J. T. Zhang, *Adv. Energy Mater.* **2019**, *9*, 1802939.

[42] M. N. Shaddad, P. Arunachalam, J. Labis, M. Hezam, A. M. Al-Mayouf, *Appl. Catal. B* **2019**, *244*, 863–870.

[43] C. Zhao, B. Liu, X. Li, K. Zhu, R. Hu, Z. Ao, J. Wang, *Chem. Commun.* **2019**, *55*, 7151–7154.

[44] T. Ivanova, A. Naumkin, A. Sidorov, I. Eremenko, M. Kiskin, *J. Electron Spectrosc. Relat. Phenom.* **2007**, *156–158*, 200–203.

[45] A. L. Kaledin, Z. Huang, Y. V. Geletii, T. Lian, C. L. Hill, D. G. Musaev, *J. Phys. Chem. A* **2010**, *114*, 73–80.

[46] A. J. Bard, M. A. Fox, *Acc. Chem. Res.* **1995**, *28*, 141–145.

[47] J. W. Boclair, P. S. Braterman, J. Jiang, S. Lou, F. Yarberry, *Chem. Mater.* **1999**, *11*, 303–307.

[48] J. W. Boclair, P. S. Braterman, *Chem. Mater.* **1998**, *10*, 2050–2052.

[49] H. Jiang, K. ichi Katsumata, J. Hong, A. Yamaguchi, K. Nakata, C. Terashima, N. Matsushita, M. Miyauchi, A. Fujishima, *Appl. Catal. B* **2018**, *224*, 783–790.

[50] O. Sato, V. Einaga, T. Iyoda, A. Fujishima, K. Hashimoto, *J. Electrochem. Soc.* **1997**, *144*, L11.

[51] Z. Y. Yu, Y. Duan, J. D. Liu, Y. Chen, X. K. Liu, W. Liu, T. Ma, Y. Li, X. S. Zheng, T. Yao, M. R. Gao, J. F. Zhu, B. J. Ye, S. H. Yu, *Nat. Commun.* **2019**, *10*, 2799.